Performance of hydrogen storage tank with TPRD in an engulfing fire

Performance of hydrogen storage tank with TPRD in an engulfing fire

Molkov, V.[1], Dadashzadeh, M.[2], Kashkarov, S.[1,*], Makarov, D.[1]

[1] Hydrogen Safety Engineering and Research Centre (HySAFER), University of Ulster, Newtownabbey, BT37 0QB, Northern Ireland, UK

[2] Efectis UK/Ireland, The Bower Stockley Park, Uxbridge, UB11 1AF

***Corresponding author: Tel.: +44-28-903-68668; Email: s.kashkarov@ulster.ac.uk**

ABSTRACT

The performance of a composite hydrogen storage tank with TPRD in an engulfing fire is studied. The non-adiabatic tank blowdown model, including in fire conditions, using the under-expanded jet theory is described. The model input includes thermal parameters of hydrogen and tank materials, heat flux from a fire to the tank, TPRD diameter and TPRD initiation delay time. The unsteady heat transfer from surroundings through the tank wall and liner to hydrogen accounts for the degradation of the composite overwrap resin and melting of the liner. The model is validated against the blowdown experiment and the destructive fire test with a tank without TPRD. The model accurately reproduces experimentally measured hydrogen pressure and temperature dynamics, blowdown time, and tank's fire-resistance rating, i.e. time to tank rupture in a fire without TPRD. The lower limit for TPRD orifice diameter sufficient to prevent the tank rupture in a fire and, at the same time, to reduce the flame length and mitigate the pressure peaking phenomenon in a garage to exclude its destruction, is assessed for different tanks, e.g. it is 0.75 mm for largest studied 244 L, 70 MPa tank. The phenomenon of Type IV tank liner melting for TPRD with lower diameter is revealed and its influence on hydrogen blowdown is assessed. This phenomenon facilitates the blowdown yet requires further detailed experimental validation.

KEYWORDS: hydrogen storage tank, blowdown, fire-resistance rating, specific heat release rate, TPRD diameter and activation time, liner melting phenomenon.

NOMENCLATURE

A_{int}	internal surface of a tank	m^2
b	co-volume constant of gas in Abel-Noble equation	m^3/kg
C_D	discharge coefficient	-
$c_{p,air}$	specific heat capacity of air	J/kg/K
$c_{p,g}$	specific heat capacity of gas at constant pressure	J/kg/K
c_{pw}	specific heat capacity of tank wall material	J/kg/K
D	diameter	m
g	gravity acceleration	m/s^2
H_d	resin heat of decomposition	J/kg
h_{out}	enthalpy going out of the tank	J/kg
k	heat transfer coefficient at a wall surface	$W/m^2/K$
L	length	m
M	molar mass	kg/mol
$\dot{m}$	entrainment mass flow rate	kg/s
m	mass	kg
n	control volume number	-
Nu_{Din}	Nusselt number inside a tank	-

P	pressure	Pa
Pr_{air}	Prandtl number of air	-
Q	heat into a system from the surroundings	J
$q"$	heat flux	W/m^2
Ra_{Din}	Rayleigh number of gas inside a tank	-
R_g	hydrogen gas constant	$m^2/s^2/K$
S	source term, thickness	$J/m^3/s$, m
T	temperature	K
t	time	s
u	velocity	m/s
U	total internal energy of gas inside a tank	J
V	tank volume	m^3
x	distance	m
Z	compressibility factor	-
λ	thermal conductivity	W/m/K
μ_g	gas dynamic viscosity	Pa·s
μ_{air}	air viscosity	Pa·s
ρ	density	kg/m^3
β	thermal expansion coefficient of gas inside a tank	K^{-1}
β_d	decomposition fraction	-
γ	specific heats ratio	-

Subscripts

air	air
amb	ambient
$b.min.$	burst minimum pressure
$CFRP$	carbon fibre reinforced polymer
$cond$	conduction
$conv$	convection
d	decomposition
ext	external
g	gas
$HDPE$	high-density polyethylene
He	helium
$H2$	hydrogen
int	internal
$int\ natural$	internal natural
$load\ b.$	load-bearing
NWP	nominal working pressure
$TPRD$	thermally activated pressure relief device
w	wall

$w(ext)$	wall external side
$w(int)$	wall internal side
$w(n)$	wall grid point “n”
1	inside the tank
2	real nozzle exit
3	notional nozzle exit

Superscript

0	initial
i	iteration

ABBREVIATIONS

BPR	burst pressure ratio
CFD	computational fluid dynamics
CFRP	carbon fibre reinforced polymer
CGH2	compressed gaseous hydrogen
CNG	compressed natural gas
COPV	composite overwrapped pressure vessel
CV	control volume
EOS	equation of state
FRR	fire-resistance rating
GTR	Global Technical Regulation
H2	hydrogen
HDPE	high-density polyethylene
HGV	heavy goods vehicle
HPV	hydrogen-powered vehicle
HRR	heat release rate
HRR/A	specific heat release rate
ISO	International Organization for Standardization
LDV	light-duty vehicle
NWP	nominal working pressure
OEM	original equipment manufacturer
PPP	pressure peaking phenomenon
RCS	regulations, codes and standards
TPRD	thermally activated pressure relief device

1. INTRODUCTION

The market of high-pressure hydrogen storage tanks for road, rail, marine, aviation, and stationary domestic and industrial applications includes mainly lightweight composite Type III (aluminium liner) and Type IV (polymer liner) tanks. There is a variety of capacities of hydrogen tanks. For instance, a passenger car could have a couple of tanks with about 5 kg of hydrogen in total [1], buses could store onboard around 50 kg and trains 100-200 kg. Hydrogen onboard storage pressure is currently 35 MPa (buses, trains, etc.) and 70 MPa (cars, trucks, etc.). The storage pressure could be

up to 95 MPa [2]. Tank volume ranges from 7.5 L to 360 L. For example, a ship hydrogen storage system [3] comprises 9x35 MPa cylinders of 8.5 kg hydrogen each, i.e. 360 L volume tanks as can be calculated using real gas equation of state (EOS).

Besides many advantages such as lightweight and strength, the main weakness of composite tanks is a reaction to fire. To prevent tank's rupture in a fire and its catastrophic consequences, i.e. blast wave, fireball and projectiles, the UN GTR#13 [4] and the EU Regulations No.134 [5], [6] assume that thermally activated pressure relief device (TPRD) is installed on hydrogen onboard storage tanks to release hydrogen and exclude rupture in a fire. However, the performance of a tank-TPRD system in a fire is not yet fully understood and thus the requirements to the comprehensive safety design of a tank-TPRD system are not yet available. This study addresses this knowledge gap.

The paper focuses on the analysis of tank-TPRD system performance in the engulfing fire only. The continuous localised fire that does not affect TPRD will result in a tank rupture early or later. Indeed, in the case of a localised fire, a TPRD may not start releasing gas being distant from high temperature. This was observed in accidents with CNG storage tanks equipped by TPRDs [7]–[9]. The scenarios when TPRD is obstructed from the fire during an accident or simply not performing due to non-zero failure probability are out of the scope of this study.

1.1. Dependence of tank FRR on HRR/A in a fire

One typical scenario of a vehicle fire is a gasoline or diesel spill fire characterised by the specific heat release rate of HRR/A=1-2 MW/m^2 [10]–[12]. For example, diesel fires in the pan with or without gravel [12] generate HRR/A=0.9 MW/m^2 and HRR/A=1.5 MW/m^2 respectively.

Another scenario is a tyre fire. The total HRR for a tyre fire in the study [12] is HRR=0.19 MW. To calculate HRR/A for vertically and horizontally placed tyre the area of the tyre projections should be calculated first, and then the specific heat release rate can be calculated as HRR/A=1.36 MW/m^2 and HRR/A=0.95 MW/m^2 respectively.

The examples above describe potential fire sources in case of arson or post-crash fire that can impact an onboard tank, e.g. when a hydrogen-powered vehicle (HPV) is overturned. The fire resistance rating (FRR), i.e. time to tank rupture in a fire without TPRD (simulation of scenarios of a localised fire, failed or blocked TPRD), of currently used tanks is 4-6 min as evidenced by experimental data [13], [14]. The FRR decreases with the increase of HRR/A and reaches a "plateau" at HRR/A>1 MW/m^2 [15]. The localised portion of the fire test of GTR#13 [4] and R134 [5] requires the hydrogen tank to withstand localised fire for 10 min before switching to the engulfing portion. Thus, the use of gasoline/diesel fire or other material fires with similar HRR/A would imply tank rupture during the localised portion of the fire test following GTR#13 and R134 protocols. There are two ways around this serious safety issue of tank rupture during the regulated localised fire test. The first solution is to increase the tank's FRR beyond 10 min or to use explosion free in fire TPRD-less tanks invented at Ulster. The second "way around" for the tank to pass the fire test is to decrease HRR/A of the fire source to the level when the tank's FRR shall exceed 10 min, e.g. to introduce the upper limit HRR/A=0.35 MW/m^2. Obviously, this "solution" could have serious safety implications in real life.

The quantitative risk assessment [16] of the use of HPVs on London roads demonstrated that the risk is acceptable if the FRR of onboard storage tanks is above 50 min, i.e. much longer than 4-6 min what unprotected storage tanks could currently provide in real fires with HRR/A>1 MW/m^2.

1.2. Dependence of hydrogen hazards on TPRD release diameter

The former "intuitive" approach, i.e. quickly release hydrogen from a tank in a fire using a comparatively large TPRD diameter of 5-6 mm to prevent its rupture, has no scientific background and brings several serious safety drawbacks. One of them is a large flame length which is known to be directly proportional to the TPRD diameter [17]. For example, the flame length from 6 mm

diameter TPRD (here and throughout the paper the TPRD diameter is considered as the minimum diameter in the release path) from 87.5 MPa storage tank is longer than 21 m. It is worth mentioning here that the "no-harm" hazard distance is 3.5 times longer than free flame length for momentum-dominated jets [17]. The second drawback of a larger diameter TPRD is the delayed ignition of a highly turbulent hydrogen jet that could generate pressure loads able to seriously injure people [17]. The third shortcoming is related to confined spaces like tunnels, underground parking, warehouses, etc. In confine space, an unignited release from a large diameter TPRD could create a flammable cloud/layer under a ceiling that, if ignited, would undergo deflagration or even transit to detonation, the last is being the worst-case scenario for hydrogen incident to be avoided by all means. Yet, there is an even more serious disadvantage of larger diameter TPRDs. This is the pressure peaking phenomenon (PPP) which is characteristic for hydrogen only compared to other fuels [18]–[22]. The ISO standard 19882:2018 [23] requires: "The adequacy of flow capacity of pressure relief devices for a given application is to be demonstrated by … the minimization of the hazardous effects of the pressure peaking phenomenon". It is known that civil structures can withstand without damage the overpressures of the order of 10 kPa. In garages with vent area of the order of brick size, the overpressure threshold of 10 kPa would not be exceeded if TPRD diameter is fractions of a millimetre.

Smaller diameter TPRDs could eliminate all four mentioned above safety concerns. This paper aims to find out a lower limit of TPRD diameter that is sufficiently "large" to exclude a tank rupture in a fire and still adequately "small" to exclude large flames, hazardous pressure loads from delayed ignition of the under-expanded jet, formation and deflagration/detonation of the flammable hydrogen-air layer in confined space, and the destructive PPP in garage-like enclosures. This aim can also be achieved by using innovative explosion free in fire TPRD-less tanks [24], but this breakthrough safety technology is the subject of another paper.

1.3. Failure mechanism of a composite tank subject to fire

The thermal behaviour of a tank-TPRD system in an engulfing fire requires an understanding of underlying physical phenomena. Hydrogen temperature and pressure inside the tank are affected by two acting in opposite directions phenomena. The blowdown decreases hydrogen temperature and pressure inside the tank. The heat transfer from fire through the tank wall increases hydrogen temperature and pressure. The heat flux from the fire increases the composite temperature and a part of this heat flux is used to decompose the resin of the wall composite starting from the external tank surface.

The composite tank failure mechanism validated in our studies is as follows. The resin decomposition front is determined by a significant resin mass loss due to the energy transferred from a fire and being partially spent on the decomposition. There are many physical and chemical processes happening to the composite material under heat flux, including glass transition, ignition, gasification, etc. For instance, the study [25] examines the complex degradation process of the composite with different fibre content. The main phenomenon that defines a tank rupture in fire is the resin mass loss and thus inability to bond fibre plies and maintain the composite material strength. In other words, when the resin is decomposed the carbon plies in these locations become "unbound" or "loose" and the composite turns not load-bearing. The regulations establish a requirement for the minimum burst pressure of carbon fibre reinforced polymer (CFRP) overwrapped tank as 2.25 times NWP. This means that the needed load-bearing wall thickness fraction to withstand pressure equal to NWP is only 1/2.25, i.e. 0.44 of the wall thickness. This fraction increases if the pressure inside the tank grows, e.g. due to hydrogen temperature increase. The tank without TPRD ruptures when moving inwards the resin decomposition front meets the moving outwards load-bearing wall thickness fraction. This represents the tank failure mechanism applied in our studies. Dadashzadeh et al. [26] modelled scenarios of non-adiabatic tank blowdown and FRR assessment of a tank without TPRD separately. Here we study a tank-TPRD system

performance in conditions when both the blowdown and fire affect the system performance simultaneously.

This study aims at the understanding of thermal behaviour of a tank-TPRD system in a fire and the development of a methodology to optimise the TPRD diameter to prevent both tank rupture in a fire and allow parking of HPVs in confined spaces like garages and maintenance shops without risk of civil structure destruction by PPP. To achieve the aim the physical model is developed and validated against non-adiabatic tank blowdown test and destructive fire test of a tank without TPRD. The model is based on the under-expanded jet theory and accounts for various parameters and phenomena known to affect the performance of a tank-TPRD system: hydrogen tank volume, storage pressure, temperature, wall and liner materials and thickness; TPRD release diameter and initiation delay time; radiative heat transfer from the fire to the tank surface, convective heat transfer from a fire to the external wall surface and from the liner to hydrogen; conductive heat transfer through the load-bearing wall and the liner; thermal degradation of the composite resin; melting of the liner, etc.

2. THE UNDER-EXPANDED JET THEORY FOR NON-ADIABATIC TANK BLOWDOWN

The under-expanded jet theory [17],[27] is used to calculate the hydrogen parameters inside a tank, at real (TPRD) nozzle exit, and notional nozzle exit during the tank blowdown. It has been intensively used to calculate flow parameters at the notional nozzle exit applied as a boundary in computational fluid dynamics (CFD) studies of hydrogen releases and dispersion to make simulation time reasonable. Previously the theory was available only for adiabatic and isothermal conditions at the internal tank wall. Here the under-expanded jet theory is expanded to the non-adiabatic formulation when a tank-TPRD system thermal behaviour is affected by both the blowdown of hydrogen and the heat transfer from the fire. Figure 1 shows schematically parts of a tank, its wall and an under-expanded jet.

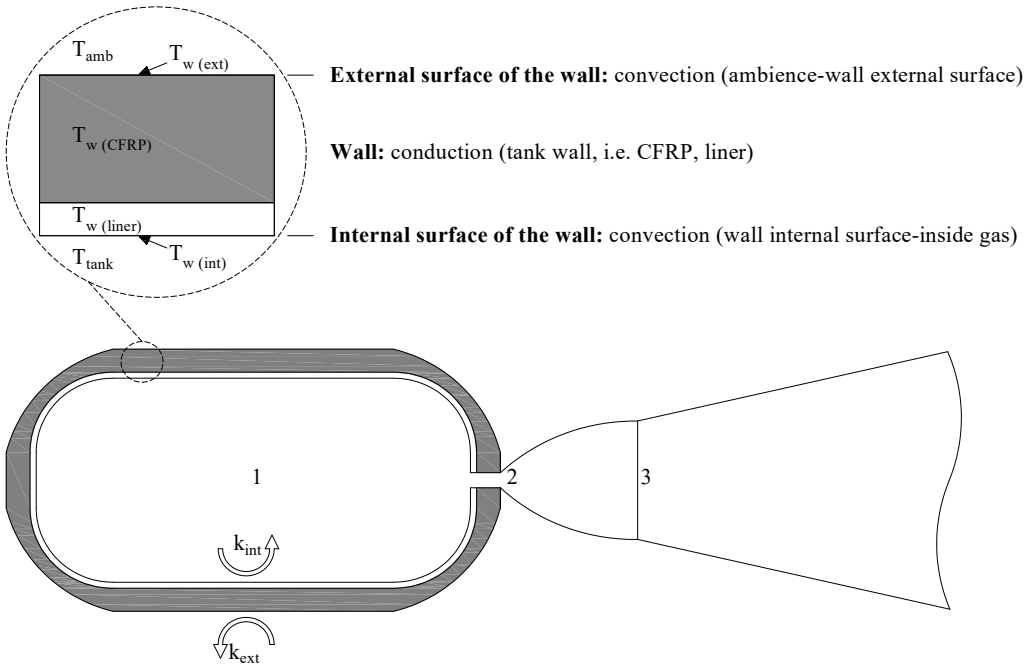

Figure 1. Schematic diagram of a pressurised tank: 1 - internal tank space, 2 - real nozzle exit (TPRD), 3 - notional nozzle exit [26].

Unsteady heat transfer equation is applied to calculate the conductive heat transfer through the tank wall using the finite-difference method [28]. The resin of the composite tank decomposes when the

local temperature exceeds the decomposition value [29]–[33]. Nusselt number correlations are applied to calculate the heat transfer coefficient for natural and forced convection [34].

Hydrogen parameters inside the tank are calculated by the Abel-Noble real gas EOS [18]:

$$P_1 = Z\rho_1 R_{H_2} T_1, \quad (1)$$

where $Z = 1/(1 - b\rho_1)$ is the compressibility factor, P_1, ρ_1 and T_1 are the pressure, density and temperature respectively.

The first law of thermodynamic is applied to bring together the rate of change of hydrogen internal energy in the tank, the rate of heat transfer to/from hydrogen through the tank wall, including liner, and the rate of enthalpy decrease due to hydrogen outflow:

$$\frac{dU}{dt} = \frac{dQ}{dt} - h_{out}\frac{dm}{dt}. \quad (2)$$

The enthalpy of real gas hydrogen flowing out of the tank is $h_{out} = c_{p,g}T_1 + bP_1$ [18]. The enthalpy equation for the Abel-Noble gas is amended here by the term "bP_1" compared to [17].

The internal energy of real gas is [35]:

$$U = \frac{P_1(V - m_1 b)}{\gamma - 1}. \quad (3)$$

The rate of convective heat transfer at the internal tank wall surface is [36]:

$$\frac{\mathrm{d}Q}{\mathrm{d}t} = k_{int}A_{int}\left(T_{w(int)} - T_1\right). \quad (4)$$

The heat transfer coefficient at the internal tank surface, k_{int}, is calculated as a function of Nusselt number, internal tank diameter, and hydrogen thermal conductivity interpolated for different pressure and temperature as [37]:

$$k_{int} = \frac{\lambda_g \times Nu_{Din}}{D_{int}}. \quad (5)$$

This study takes into account only natural convection for the internal tank surface. This is based on the conclusion of the study [34] that unlike the filling of a tank where a mixed convection regime (forced and natural) is suitable, in the case of discharging a tank, the application of natural convection provides a better model performance. Natural convection Nusselt number, Nu_{Din}, is calculated by the empirical equation [34]:

$$Nu_{Din} = 0.104 \times \left(\frac{g\beta|T_1 - T_{w(int)}|c_{p,g}(\rho_1)^2 D_{int}^3}{\mu_g \lambda_g}\right)^{0.352}. \quad (6)$$

Differentiating Eq. (3) and considering the heat transfer rate defined by Eq. (4), the differential equation for calculation of hydrogen pressure in the tank, P_1, can be derived from Eq. (2) as:

$$\frac{\mathrm{d}P_1}{\mathrm{d}t} = \frac{\frac{dm}{dt}\cdot\left(\frac{P_1}{\gamma-1} - c_{p,g}\cdot T_1 - bP_1\right) + k_{int}A_{int}\left(T_{w(int)} - T_1\right)}{\frac{V - m_1 \cdot b}{\gamma - 1}}. \quad (7)$$

The temperature of hydrogen inside the tank in the assumption of uniformity is:

$$T_1 = \frac{P_1(1 - b\rho_1)}{\rho_1 R_{H_2}}, \quad (8)$$

where the density is calculated as $\rho_1 = \frac{m_1}{V}$.

Hydrogen density at the real nozzle exit, ρ_2, is calculated by solving the transcendental equation of isentropic expansion [17]:

$$\left[\frac{\rho_1}{1 - b\rho_1}\right]^{\gamma} = \left[\frac{\rho_2}{1 - b\rho_2}\right]^{\gamma} \cdot \left[1 + \left(\frac{\gamma - 1}{2(1 - b\rho_2)^2}\right)\right]^{\gamma/\gamma - 1}. \quad (9)$$

Hydrogen temperature at the real nozzle exit is calculated using the energy conservation equation [17]:

$$\frac{T_1}{T_2} = 1 + \frac{\gamma-1}{2(1-b\rho_2)^2}. \quad (10)$$

The Abel-Noble EOS [18] is used to calculate the pressure at the real nozzle exit:

$$P_2 = \frac{\rho_2 R_g T_2}{1-b\rho_2}. \quad (11)$$

Due to choked flow conditions, hydrogen velocity at the real nozzle exit is equal to the local sound velocity [17],[18]:

$$u_2 = \frac{(\gamma R_g T_2)^{0.5}}{1-b\rho_2}. \quad (12)$$

The energy conservation equation [17],[27] is employed to calculate hydrogen temperature at the notional nozzle exit:

$$T_3 = \frac{2T_2}{\gamma+1} + \frac{(\gamma-1)}{(\gamma+1)} \cdot \frac{P_2}{\rho_2(1-b\rho_2)R_g}. \quad (13)$$

Hydrogen pressure at the notional nozzle exit is assumed to be equal to the ambient pressure, P_{amb}. Hydrogen density at the notional nozzle exit is then:

$$\rho_3 = \frac{P_{amb}}{P_{amb}b+R_g T_3}. \quad (14)$$

Hydrogen velocity at the notional nozzle exit is equal to the local speed of sound [17],[27]:

$$u_3 = \frac{(\gamma R_g T_3)^{0.5}}{1-b\rho_3}. \quad (15)$$

The mass conservation equation between the real and notional nozzle exits is applied to calculate the diameter of the notional nozzle:

$$D_3 = D_2\sqrt{C_D \frac{\rho_2 u_2}{\rho_3 u_3}}, \quad (16)$$

where D_2 is the real nozzle exit diameter, D_3 is the notional nozzle exit diameter, and C_D is the discharge coefficient, which accounts for friction and minor losses in the flow path from the tank to the atmosphere affecting the mass flow rate from the system.

The mass flow rate is then:

$$\dot{m} = \frac{\rho_3 u_3 \pi (D_3)^2}{4}. \quad (17)$$

The mass flow rate is updated at each time step and then is used as input to Eq. (7).

The model solves the unsteady heat conduction equation through the tank wall that can be found elsewhere [28]:

$$\rho_w c_{pw} \frac{dT_w}{dt} = \frac{d}{dx}\left(\lambda_w \frac{dT_w}{dx}\right) + S. \quad (18)$$

The heat of resin decomposition is introduced into the energy sink term, S. This heat is consumed within the range of decomposition temperatures [38]. The source term is implemented following [29]–[33]:

$$S = -\rho_w \beta_d \frac{dH_d}{dt}, \quad (19)$$

where β_d is the decomposition factor, H_d is the resin decomposition heat. The decomposition factor β_d varies between 0 and 1 in each CV, and is governed by the following conditions: $\beta_d = 0$ if $T_{w(n)} < T_{d1}$ or $T_{w(n)} > T_{d2}$, and $\beta_d = 1$ if $T_{d1} \le T_{w(n)} \le T_{d2}$. Here T_{d1} and T_{d2} are the initial and final temperatures of the resin decomposition range, respectively. The energy sinks in the CV while β_d=1. The rate of the decomposition heat change, $\frac{dH_d}{dt}$, can be expressed through the decomposition temperature range:

$$\frac{dH_d}{dt} = \frac{dT_w}{dt} \cdot \frac{H_d}{T_{d2}-T_{d1}}. \quad (20)$$

The boundary conditions at internal and external tank surfaces are respectively:

$$q_{cond}^{"}\ (internal) = q_{conv}^{"} \Rightarrow \lambda_w \frac{dT_{w\,(n)}}{dx}\Big|_{n=int} = k_{int}\left(T_1 - T_{w\,(int)}\right), \quad (21)$$

$$q_{cond}^{"}\ (external) = q_{conv}^{"} \Rightarrow -\lambda_w \frac{dT_{w\,(n)}}{dx}\Big|_{n=ext} = k_{ext}\left(T_{w\,(ext)} - T_{amb}\right). \quad (22)$$

The external convective heat transfer coefficient, k_{ext}, does not have a significant effect on the heat transfer [28],[39]. For the model validation against the blowdown experiment without fire, k_{ext}=6 W/m^2/K is accepted in Eq. (22) [39].

The heat flux from the fire to the tank in our study is extracted from 3D simulations of the tank located in a fire with characteristic for gasoline/diesel fire HRR/A=1 MW/m^2. The maximum heat flux was located on the dome part of the tank. The heat flux (in W/m^2) as a function of time (in seconds) for HRR/A=1 MW/m^2 (similar dependencies for other HRR/A measured in the validation experiment are presented further in this paper) is:

$$q" = (-11.81 \cdot \ln(t) + 113.97) \cdot 10^3. \quad (23)$$

The heat flux on the dome part was selected as it was the largest in the simulations, which is due to the thinnest wall thickness at the tank dome (this is an example of improper tank design related to fire resistance). The use of q" allows simplifying Eq. (22) for cases with external fire to:

$$q_{cond}^{"}\ (external) = q_{conv}^{"} \Rightarrow \quad -\lambda_w \frac{dT_{w\,(n)}}{dx}\Big|_{n=ext} = q". \quad (24)$$

The system of equations is solved iteratively. Initial conditions (iteration number $i = 0$) are:

$\dot{m}^0 = 0$,

$\rho_1^0 = \frac{P_1^0}{P_1^0 \cdot b + R_g \cdot T_1^0}$,

$m_1^0 = V \cdot \rho_1^0$,

$$Nu_{int}^0 = 0.104 \times \left(\frac{g\beta\left|T_1^0 - T_{w(int)}^0\right| c_{p,g}\left(\rho_1^0\right)^2 D_{int}^3}{\mu_g \lambda_g}\right)^{0.352},$$

$k_{int\ natural}^0 = \frac{\lambda_g \cdot Nu_{int\ natural}^0}{D_{int}}$.

Table 1 shows the model input parameters.

Table 1. Input parameters, calculation procedure and output parameters of the model.

Input parameters	
V, b, γ, T_{amb}, P_{amb}, $q"$, T_1^0, T_w^0, P_1^0, A_{int}, Δx, Δt, R_g, M_g, $\rho_{w(n)}$, $c_{p\,w(n)}$, λ_w, k_{ext}, C_D, D_{int}, D_{out}, g, β, T_w^0, k_{int}^0, $c_{p,g}$, μ_g, λ_g, ρ_1^0, m_1^0, $q"$, S_{HDPE}, S_{CFRP}, H_d, T_{d1}, T_{d2}	
Calculation procedures	
Iteration steps	**Output parameters**
1	Hydrogen mass in a tank, ($m_1^i = m_1^{i-1} + \left(\frac{dm}{dt}\right)\Delta t$)
2	Hydrogen density, $\rho_1 = \frac{m_1}{V}$
3	Pressure change ($\frac{dP_1}{dt}$), Eq. (7)
4	Hydrogen pressure (P_1), $P_1^i = P_1^{i-1} + \left(\frac{dP_1}{dt}\right)\Delta t$
5	Hydrogen temperature (T_1), Eq. (8)
6	Hydrogen density at real nozzle exit (ρ_2), Eq. (9)

7	Hydrogen temperature at real nozzle exit (T_2), Eq. (10)
8	Hydrogen pressure at real nozzle exit (P_2), Eq. (11)
9	Hydrogen velocity at real nozzle exit (u_2), Eq. (12)
10	Hydrogen temperature at notional nozzle exit (T_3), Eq. (13)
11	Hydrogen density at notional nozzle exit (ρ_3), Eq. (14)
12	Hydrogen velocity at notional nozzle exit (u_3), Eq. (15)
13	Notional nozzle exit diameter (D_3), Eq. (16)
14	Mass flow rate ($\dot{m} = \frac{dm}{dt}$), Eq. (17)
16	Transient temperature within tank wall (T_w), Eq. (18)
17	Wall (liner in this study) internal surface temperature ($T_{w\,(int)}$), Eq. (21)
18	Wall external surface temperature ($T_{w\,(ext)}$) Eq. (22) for blowdown without fire Eq. (24) for blowdown in fire conditions
20	Heat transfer coefficient at the internal wall surface (k_{int}), Eq. (5)
21	Repeating steps 1 to 20 if P_1/P_{amb} > 1.9. else simulation is stopped.

The model simulates the dynamics of hydrogen pressure and temperature inside the tank, the temperature profile within the load-bearing wall and the liner, the tank blowdown time without and with the fire, the FRR.

3. THE MODEL VALIDATION

3.1. Validation against the blowdown experiment

The blowdown validation experiment was carried out at the Karlsruhe Institute of Technology (KIT) [26]. The impinging jet test platform was used with a high-pressure Type IV tank of volume 19 L connected to a release nozzle of 1 mm diameter. The vessel was filled to 70 MPa by helium and then cooled down to room temperature (293 K) before the test. Table 2 presents the tank characteristics. The temperature dynamics inside the tank was measured by a thermocouple installed in the middle of the tank. Pressure dynamics inside the tank was also measured during the test.

Table 2. Dimensions and properties of the 19 L, 70 MPa tank used in the blowdown validation experiment and as input in the simulations.

Parameter	Value	Reference
Tank dimensions		
V, L	19	[40]
D_{int}, mm	180	[40]
D_{out}, mm	228	[40]
L, mm	0.904	[40]
HDPE liner		
S_{HDPE}, mm	**7**	[38]
λ, W/m/K	0.385	[41]
c_p, J/kg/K	1584	[41]
ρ, kg/m^3	945	[41]

CFRP structural layer		
S_{CFRP}, mm	17	[38]
λ, W/m/K	0.5	[42]
c_p, J/kg/K	1020	[42]
ρ, kg/m^3	1360	[42]

Table 3 shows the input parameters used to perform the helium blowdown validation experiment simulations.

Table 3. Input parameters for the blowdown validation experiment simulations.

Parameter	Value	Reference
$c_{p,g}$, J/kg/K	Interpolated function	[43]
λ_g, W/m/K	Interpolated function	[43]
β, 1/K	Interpolated function	[43]
R_{He}, Nm/kg/K	2080	[43]
γ_g	1.66	[43]
b, m^3/kg	$2.67 \cdot 10^{-3}$	[44]
M_g, g/mol	4.003	[43]
g, m/s^2	9.81	Acceleration of gravity
T_{amb}, K	293	Assumption
P_{amb}, Pa	$1.01 \cdot 10^{5}$	Assumption
T_1^0, K	293	KIT experiment
P_1^0, Pa	$7.00 \cdot 10^{7}$	KIT experiment
ρ_1^0, kg/m^3	$8.80 \cdot 10^{1}$	Eq. (29)
m_1^0, kg/m^3	1.67	Eq. (30)
μ_{air}, Pa·s	$1.98 \cdot 10^{-5}$	[45]
$c_{p,air}$, J/kg/K	$1.01 \cdot 10^{3}$	[45]
λ_{air}, W/m/K	$2.57 \cdot 10^{-2}$	[45]
ρ_{air}, kg/m^3	1.21	[45]

Figure 2a compares the measured and simulated pressure transients. Results calculated by both the former adiabatic blowdown model [27] and the non-adiabatic blowdown model described in this paper are presented. The presented in Table 2 and 3 tank parameters and gas properties were used in the simulations. Figure 2b shows experimental and simulated temperature dynamics.

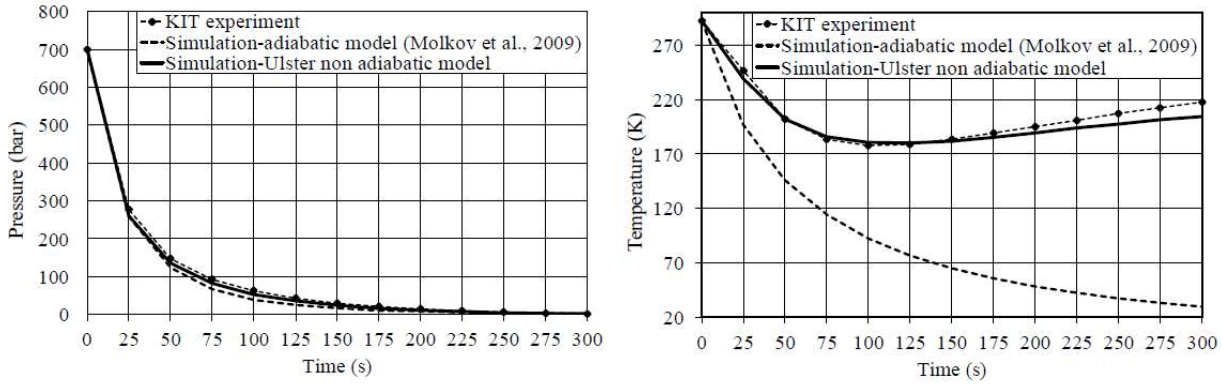

(a) (b)

Figure 2. Measured and simulated pressure (a), and temperature (b) in the 19 L, 70 MPa Type IV tank.

The simulated by both models pressure do not differ significantly. Yet, the non-adiabatic model reproduces the pressure closer to the experiment. However, there is a drastic difference in the temperature dynamics simulated by the two models. The adiabatic model shows that in the absence of heat transfer from the surroundings through the tank wall to hydrogen, the hydrogen temperature drops in 5 min down to an unrealistic 33 K (Fig. 2b). Contrary, the non-adiabatic model closely reproduces measured temperature dynamics, including the characteristic temperature minimum, with a deviation from measured temperature within 6%.

3.2. Validation against the fire test (tank without TPRD)

The two destructive fire tests with identical 36 L Type IV hydrogen tanks filled with a pressure equal to NWP=70 MPa were performed at KIT within the EU H2FC research infrastructure project. Table 4 shows the tank parameters and thermal properties of the composite and the liner.

The premixed methane-air burner with HRR/A=0.62 MW/m^2 was used inside the large enclosure [46]. The heat flux from the fire to the tank in this validation experiment is defined by 3D simulations as q"=3.8 · $10^{-5}t^2$-6.6 · $10^{-2}t$+50161. To exclude hydrogen reaction with air after the tank rupture, the enclosure was filled with nitrogen. The FRR was 8 min 3 s for the new tank and 9 min 42 s for the "old" tank (passed cycling test), respectively.

Table 4. Tank parameters and thermal properties of liner and composite in the destructive fire tests.

Parameter	Value	Reference
Dimensions		
V, L	36	[47]
D_{in}, mm	262	[47]
D_{out}, mm	325	[47]
L, mm	910	[47]
HDPE liner		
S_{HDPE}, mm	5.27	[48]
λ, W/m/K	0.4@293 K, 0.2@423 K*	[49]
c_p, J/kg/K	2000@293 K, 2600@423 K*	[49]
ρ, kg/m^3	940	[49]
CFRP structural layer		

S_{CFRP}, mm	22.26	[48]
λ, W/m/K	Correlation	[38]
c_p, J/kg/K	Correlation	[38]
ρ, kg/m3	1360	[42]
H_d, J/kg	$3.50 \cdot 10^5$	[50]
T_d, K	554-683	[38]

Note: * - linear function applies within the specified ranges.

It is worth noting that the 36 L tank had a different wall and liner thickness in the dome part and the cylindrical part of the tank: dome part had a liner thickness of 5.27 mm and CFRP thickness of 22.26 mm; the sidewall part had a thinner liner of 3.8 mm and thicker load-bearing wall of 27.75 mm [15],[47],[48],[51]. Thus, the dome part of this tank defines the FRR. This was confirmed by 3D CFD simulations. In the dome, the thinner composite is sufficient to provide the same mechanical strength as the thicker cylindrical part due to mainly helically wound layers of the composite layup. To connect the liner and the metal boss, liner thickness tends to increase in this part. The tank developers and manufacturers should pay attention that the thickness of the composite wall should be the same throughout the tank surface to account for the tank's proper performance in a fire not only in the burst test.

The regulations require that the minimum burst pressure to NWP ratio is 2.25, i.e. $P_{b.min.}$=2.25×70 MPa=157.5 MPa. The fraction of the wall thickness that can bear NWP=70 MPa is, as was mentioned above, 1/2.25=0.44. This makes the wall thickness fraction that able to bear an extra load, hereafter referred to as "load+", as 1-0.44=0.56 at NWP.

In fire conditions, hydrogen temperature inside the tank grows. Consequently, the pressure increases above initial NWP=70 MPa forcing the load-bearing wall thickness fraction to increase, i.e. move outwards. Thus, the "load+" fraction of the wall thickness decreases. The fire degrades the composite resin starting from the tank external surface. The resin degradation front moves inwards. The failure mechanism that is applied in our studies assumes that the composite structural integrity is lost and a tank ruptures when the resin decomposition front meets the transient load-bearing fraction of the wall thickness. The model calculates how the load-bearing wall thickness fraction and the resin decomposition front move towards each other and the time when they meet, i.e. time of tank rupture (FRR). Alternatively, they may not meet, e.g. as a result of hydrogen release through TPRD or by other proven means that exclude tank rupture, e.g. the explosion free in a fire TPRD-less tanks.

There is a number of other known mechanisms applied for analysis of mechanical failures of composite, especially when using the finite element method. Those include such theories as maximum principal stress, equivalent stress, maximum principal elastic, equivalent strain theory etc [52]. This would require many complications such as hoop and helical winding patterns, fibre orientation etc. Ulster's model in turn, shows a reasonable accuracy with inclusion of other substantial physical phenomena necessary, as will be demonstrated further in this paper.

Table 5 presents the input parameters used in the model for hydrogen and ambient air properties to simulate the FRR of tanks in the destructive validation fire tests (tank parameters and properties are given in Table 4).

Table 5. The model input parameters for destructive fire tests simulations.

Parameter	Value	Reference
$c_{p,g}$, J/kg/K	Interpolated function	[37]

λ_g, W/m/K	Interpolated function	[37]
β, 1/K	Interpolated function	[37]
R_{H_2}, J/kg/K	4124.24	[37]
γ_{H_2}	1.41	[37]
b, m^3/kg	$7.69 \cdot 10^{-3}$	[44]
M_{H_2}, g/mol	2.016	[37]
T_{amb}, K	308	Assumption
P_{amb}, Pa	$1.01 \cdot 10^5$	Assumption
T_1^0, K	308	KIT experiment
P_1^0, Pa	$7.01 \cdot 10^7$	KIT experiment
ρ_1^0, kg/m^3	$3.87 \cdot 10^1$	Eq. (29)
m_1^0, kg/m^3	1.39	Eq. (30)

Figure 3a compares the experimental and simulated pressure transients during the destructive fire test. Figure 3b shows experimental and simulated temperature dynamics inside the tank. Both the pressure and the temperature calculated by the model are in good agreement with the experiment [46].

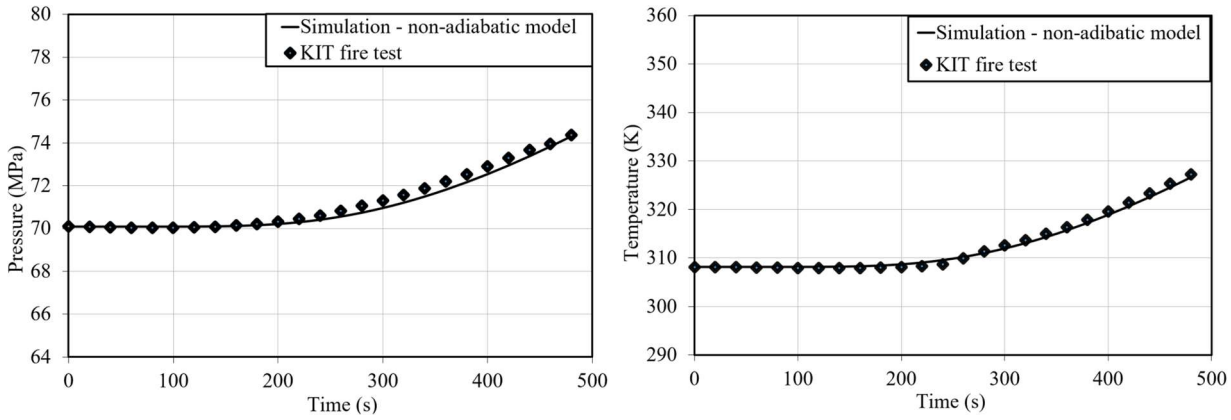

(a) (b)

Figure 3. Experiment and simulated pressure (a) and temperature (b) dynamics during the destructive tank fire test.

Figure 4 shows two experimental FRR, i.e. FRR=8 min 3 s (new tank) and FRR=9 min 42 s (used tank), and the simulated by model FRR=530 s (8 min 50 s). The calculated FRR is just between the two experimental values of FRR. It is worth noting that the resin decomposition front is represented on the graph by the lower value of the resin decomposition temperature range, T_{d1}, (red curve).

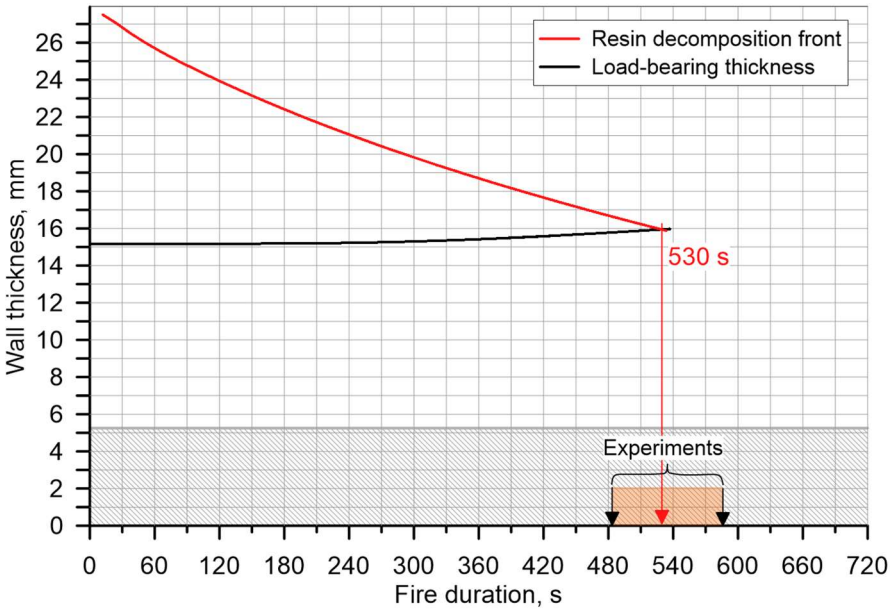

Figure 4. Two experimental [46] and simulated FRR.

4. THE UNIVERSAL DEPENDENCE OF FRR ON HRR/A

The HRR in a fire affects the FRR of a tank [15]. The specific heat release rate HRR/A, i.e. the heat release rate divided by the fire area, is a more universal parameter for scaling and comparison of different fire sources. The higher is the HRR/A the higher is the heat flux into the tank wall. The higher heat flux accelerates resin decomposition and this results in a shorter time to tank rupture (FRR). Figure 5 shows the universal dependence of the FRR on the specific heat release rate HRR/A. The FRR decreases with the increase of HRR/A and reaches a horizontal asymptote or "plateau" of 4-6 min at HRR/A>1-2 MW/m^2. This is exactly the HRR/A characteristic for fires with a spill of gasoline/diesel.

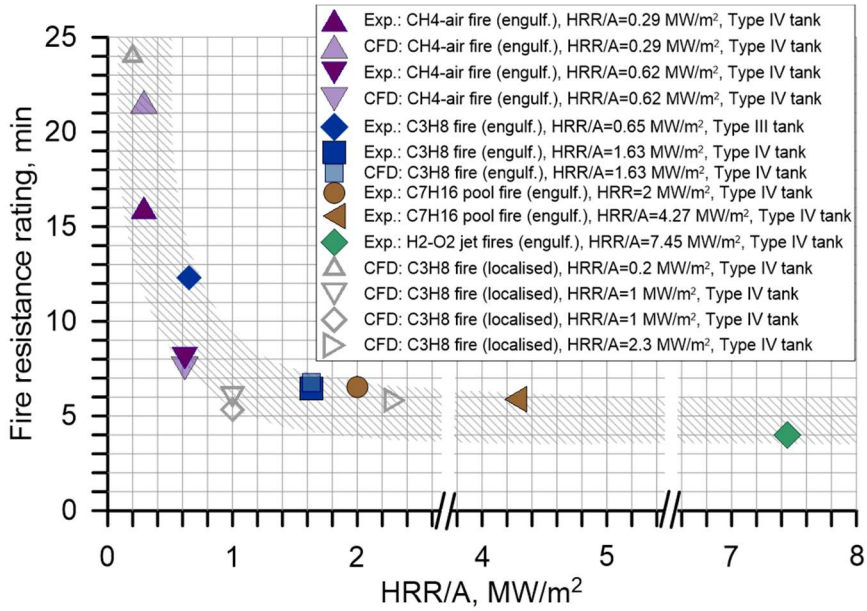

Figure 5. The FRR as a function of HRR/A [13]-[15], [46], [48], [53]-[55].

The experimental FRR points at HRR/A=0.29 MW/m^2 and HRR/A=0.62 MW/m^2 are obtained for 36 L and 70 MPa Type IV tanks in engulfing fire tests with a premixed methane-air (CH_4-air) burner in the closed facility filled in by nitrogen [46]. Previously performed CFD simulations of these two tests are shown by light purple triangles.

The experimental FRR points with propane (C_3H_8) diffusion burner and HRR/A=0.65 MW/m^2 and HRR/A=1.63 MW/m^2 are obtained in the USA engulfing fire tests with under-vehicle (88 L, 35 MPa) and stand-alone (72.4 L, 35 MPa) tanks respectively [14],[53]. The stand-alone Type IV tank fire test is well reproduced numerically (blue square). No simulations of FRR of the in-situ tank were performed due to the absence of experimental details on the geometry and location of the tank and a burner in USA test.

The experimental FRR points with n-heptane (C_7H_{16}) engulfing pool fires at HRR/A=2 MW/m^2 and HRR/A=4.27 MW/m^2 are derived from the fire tests with 36 L and 100 L Type IV tanks with NWP=70 MPa respectively [54],[55].

The numerical experiments with the propane localised fire source and 36 L, 70 MPa Type IV tank at HRR/A=0.2-2.3 MW/m^2 (hollow light grey symbols) are in agreement with the experimentally observed dependence of the FRR on the HRR/A.

The experimental FRR point with premixed hydrogen-oxygen (H_2-O_2) jet fires affecting the tank at HRR/A=7.45 MW/m^2 is for 36 L, 70 MPa Type IV tank [13] (green diamond symbol). The FRR test with hydrogen jet fires affecting the tank ultimately confirms the universal character of the revealed correlation between the FRR and the HRR/A [13].

Figure 6 shows the progression in time of the resin decomposition front and the increase of the load-bearing wall thickness fraction (proportional to the increase of pressure inside the tank). These were calculated by the presented in this paper model for 36 L, 70 MPa Type IV tank in fires of three different HRR/A: 1 MW/m^2, 0.62 MW/m^2 and 0.29 MW/m^2. For the HRR/A=0.29 MW/m^2 fire the heat flux derived from 3D CFD simulations is $q" = 2\cdot 10^{-11}t^5 - 8\cdot 10^{-8}t^4 + 1\cdot 10^{-4}t^3 - 0.0288t^2 - 24.69t + 30624$ ($q"$ for fires with two other HRRR/A are given above). Figure 6 demonstrates that the FRR is decreasing with the increase of HRR/A: FRR=836 s for HRR/A=0.29 MW/m^2, FRR=554 s for HRR/A=0.62 MW/m^2, FRR=411 s for HRR/A=1 MW/m^2. In these 3 numerical tests, the initial hydrogen temperature was 293.15 K and the pressure was 70 MPa. It is worth noting that these initial conditions slightly differ from those in the KIT experimental fire test with HRR/A=0.62 MW/m^2, i.e. 308 K and 70.1 MPa respectively, as also indicated in Table 5. For this reason, the FRR=530 s in the validation simulations (Figure 4) is by 24 s lower than the FRR=554 s for the same HRR/A in Figure 6.

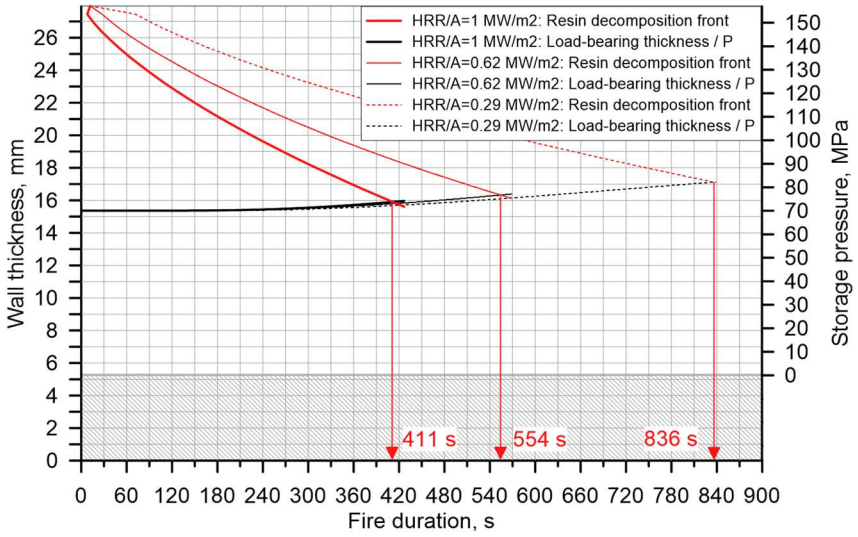

Figure 6. Location of the resin decomposition front (descending lines), load-bearing wall thickness fraction (ascending lines, left y-axis), the pressure (ascending lines, right y-axis) and the FRR values in seconds for fires of three different intensities: HRR/A=1 MW/m^2, 0.62 MW/m^2 and 0.29 MW/m^2 (36 L, 70 MPa Type IV tank without TPRD).

Figure 6 demonstrates that the increase in fire intensity (HRR/A) significantly increases the rate of resin decomposition and thus reduces the time to rupture (FRR). The standard fire test protocol must account for this observation. The absence of HRR/A control in the previous fire test protocol is a reason for poor fire test reproducibility. Control of HRR/A in fire test cannot be substituted by fire temperature control around the tank as this could implicitly reduce HRR/A in standard fire test below HRR/A in realistic gasoline/diesel fires. Opposite to the strong changes in the decomposition front propagation velocity, only a slight increase of the pressure growth in the tank and thus load-bearing wall thickness fraction propagation outwards is observed for HRR/A changes in the wide range 0.29-1.00 MW/m^2.

Thus, the development of a fire test protocol based on the control of temperature around the tank only and ignoring the role of HRR/A on the FRR is ill-posed in our opinion. This may bring serious safety concerns for the public. For example, from three considered fires only the fire test with HRR/A=0.29 MW/m^2 will allow passing the localised fire test which requires the tank not to rupture for 10 min (600 s) until TPRD is initiated after extending the fire to engulfing part. Indeed, in fires with HRR/A=1 MW/m^2 and 0.62 MW/m^2, the tank will rupture during the localised portion of the fire test of 10 min duration before the TPRD will be initiated after switching to the engulfing fire.

The right y-axis in Figure 6 shows the storage pressure. It effectively indicates the CFRP load-bearing wall thickness fraction (left y-axis). The right y-axis starts from the value "0" on the border between the liner and CFRP (the liner does not carry any load). The storage pressure 70 MPa corresponds to the wall thickness fraction holding the NWP, i.e. 1/2.25=0.44, where 2.25 is the regulated CFRP vessel's burst pressure ratio (BPR). The whole wall thickness of 27.75 mm holds 2.25x70 MPa=157.5 MPa (see left and right y-axis in Fig. 6 respectively).

5. TANK BLOWDOWN DYNAMICS WITHOUT AND WITH FIRE

Figure 7a shows the dynamics of the load-bearing wall thickness fraction for the 36 L, 70 MPa tank equipped with TPRD of 1 mm diameter. Here, TPRD release is initiated simultaneously with the fire of HRR/A=1 MW/m^2. In this example, the presence of fire practically does not affect the dynamics of the comparatively fast decrease of the load-bearing wall thickness fraction (left y-axis) due to the decrease of pressure during the blowdown (the same curves show the dynamics of pressure drop, right y-axis). The simulations demonstrated that after 605 s, when hydrogen pressure in the tank is already atmospheric, the liner melted through its entire depth.

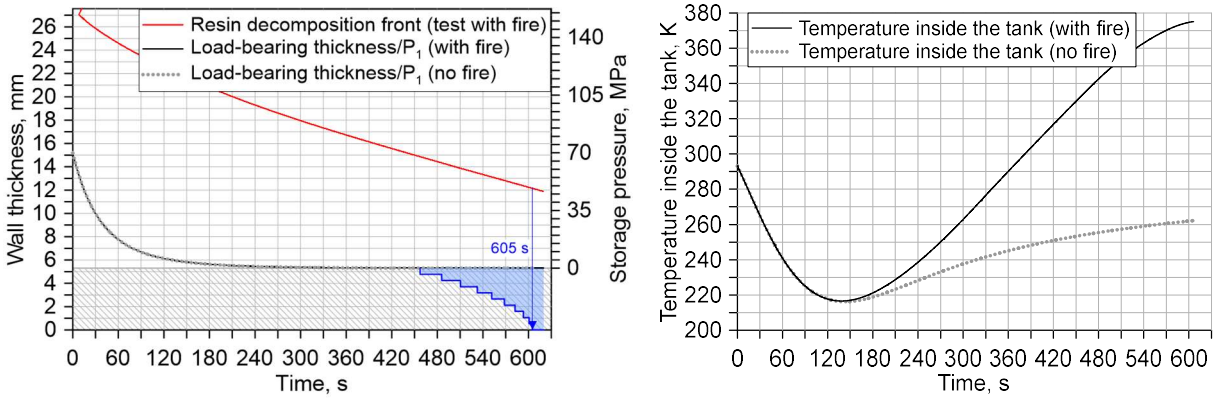

(a) (b)

Figure 7. Blowdown dynamics of 36 L, 70 MPa Type IV tank through TPRD of D_{TPRD}=1 mm without and with fire at HRR/A=1 MW/m^2. (a) – load-bearing wall thickness fraction (without and with fire, left y-axis), hydrogen pressure (right y-axis) and resin decomposition front (with fire) dynamics, (b) - hydrogen temperature dynamics.

Figure 7b demonstrates that the presence of fire does not affect the temperature decrease dynamics in the tank during about the first 2.0-2.5 minutes. This time is required for heat to be transferred through the wall and liner to hydrogen. After this time hydrogen temperature reaches its minimum and then increases faster in the presence of fire as expected. The difference reaches 113 degrees when the simulation ends at 605 s when the liner fully melts in the test with fire. In this particular example, the melting of the liner does not make any effect as the pressure inside the tank is already atmospheric.

6. VARIATION OF WALL THICKNESS WITH TANK DIAMETER

Table 6 shows the parameters of five tanks with NWP=70 MPa based on published data (except some data of 244 L tank). To study the performance of the 244 L tank we obtained its wall thickness through the analysis of ratios of tank external diameter, D_{ext}, over composite wall thicknesses, S_{CFRP}. It appeared that in 4 tanks, volumes of which varied between 7.5 L and 69.5 L, the averaged ratio D_{ext}/S_{CFRP} was found to be 15.45±3.75. The scatter ±26% can be explained by the fact that the BPR 2.25 for CFRP overwrapped tanks is the minimum requirement of the regulations to the ratio of the burst pressure to NWP and tank manufacturers are free to manufacture tanks with larger BPR. The close to averaged D_{ext}/S_{CFRP}=15.9 was taken to determine the composite wall thickness for the 244 L tank, which totalled 33.36 mm. This thickness is used in our study. We assume in our study that in each tank, except in a 36 L tank, the thicknesses of the sidewall and the dome part are equal. It is worth noting, that from 36 L tank geometry we know that the composite in the dome part is thinner, which in our opinion is improper from a fire-resistance point of view.

Table 6. Dimensions and properties of five 70 MPa tanks.

Parameters	**Tank#1** [56]	**Tank#2** [15],[47],[51]	**Tank#3** [57]	**Tank#4** [56]	**Tank#5**
V, L	7.5	36	62.4	69.5	244 [2]
D_{ext}, mm [1]	186	325	437	457	530 [2]
L, mm	521	909	748	719	2154 [2]
S_{CFRP}, mm [1]	12.7	27.75	24.3	23.8	33.36 [2]
S_{HDPE}, mm [1]	3.56	3.8	3	4.83	3 [3]
D_{ext}/S_{CFRP}	14.646	11.712	17.984	19.202	15.885 [4]
L/D_{ext}	2.8	2.8	1.7	1.6	4.1

Note: [1] - data given for tank sidewall (cylindrical) part; [2] - assumption: composite thickness obtained from the close to average ratio D_{ext}/S_{CFRP}=15.9; [3] - assumption; [4] - average D_{ext}/S_{CFRP} (sidewall) ratio.

7. METHODOLOGY TO ASSESS FIRE PERFORMANCE OF TANK-TPRD SYSTEM

Figure 5 above demonstrates that in fire conditions with HRR/A=1-2 MW/m^2 characteristic for gasoline/diesel fire a tank could rupture as short as in 4 min. The TPRD must be initiated before this time. Thus, the parametric study is performed for the conservative delay time of TPRD initiation of 3 min. Any faster TPRD activation will make the performance of the tank-TPRD system safer. Any longer TPRD initiation time is not acceptable to exclude a risk of tank rupture. To be on the conservative side and account for gasoline/diesel fires, HRR/A=1 MW/m^2 is applied in this parametric study. Tanks of Type IV with NWP=70 MPa and HDPE liner are considered here and thus the calculations results in this work cannot be directly applied to other liner and composite wall materials. The liner thickness can be seen on graphs for each of the three tanks considered in this section. The methodology applied here for three tanks of volume 244 L, 62.4 L, 36 L can be applied to an arbitrary tank-TPRD system. For consistency, in this parametric study we assume that liners

in all tanks are made of HDPE, the composite overwraps are fully made of the same CFRP and thermal properties of all tanks' materials are the same, as per Table 4 and Table 5. The initial tanks' temperature and pressure in the numerical tests are assumed to be 293 K and 70 MPa respectively.

7.1. Case of 244 L tank-TPRD system

Figure 8 shows the propagation of the resin decomposition front, load-bearing wall thickness fraction (left y-axis) related to hydrogen pressure (right y-axis) and the liner melting front (blue colour steps) in the three numerical fire tests with HRR/A=1 MW/m^2 for 244 L, 70 MPa tank-TPRD system for three different TPRD diameters: 0.5 mm, 0.75 mm, 1 mm. The system with the smallest TPRD diameter of 0.5 mm ruptures at 1457 s (24 min 17 s) when the resin decomposition front meets the load-bearing wall thickness fraction "front" (just before the liner melting through the entire depth). The system does not rupture if the TPRD diameter is equal to or larger than 0.75 mm until the full liner melting, which can be considered as an "additional" channel of hydrogen release. See section 7.4 on the effect of liner melting on the blowdown dynamics.

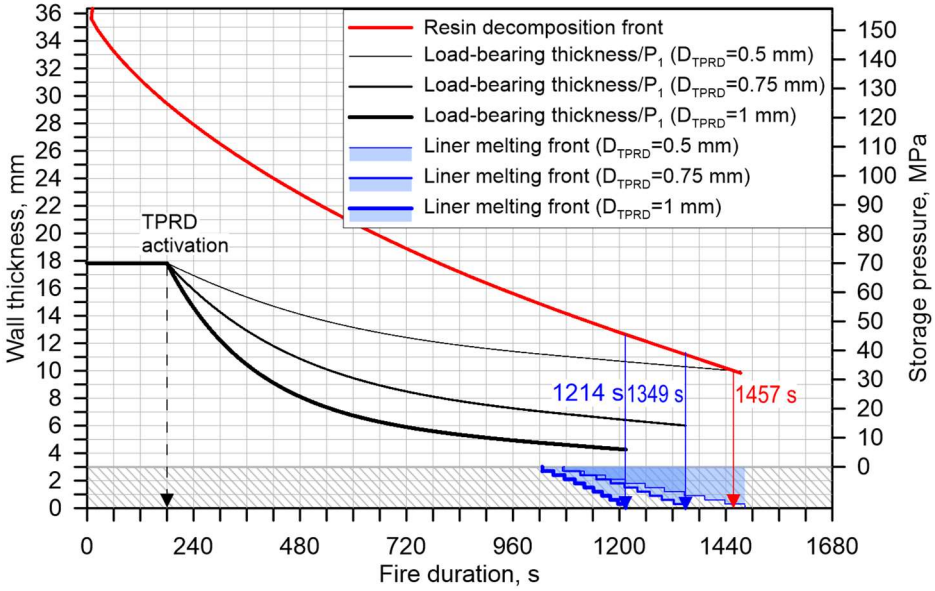

Figure 9. Performance of 244 L, 70 MPa tank-TPRD system in a fire with HRR/A=1 MW/m^2 for three different TPRD diameters: 0.5 mm, 0.75 mm, 1 mm.

The study allows insights into the thermal behaviour of the tank equipped by TPRD of comparatively small diameter. The performance of the tank-TPRD system is not trivial. For 0.75 mm TPRD when the pressure (right y-axis) drops to about 14 MPa at 1349 s, the liner melts through its depth. For TPRD of 1 mm, the liner fully melts at 1214 s when the pressure drops to about 6 MPa. The melting of the liner allows hydrogen to leak through the wall in addition to the release through TPRD.

It is worth mentioning the following published experimental observations. When the initial pressure inside a Type IV tank is substantially less than NWP the tank will leak and not burst in the fire [58]. For example, a series of fire tests were performed with 36 L tanks of NWP=70 MPa but with different initial pressure in the range of 10-70 MPa. Two tanks with initial pressure 70 MPa (100% NWP) and 52.5 MPa (75% NWP) ruptured in a fire but two other tanks with initial pressure 25 MPa (36% NWP) and 10 MPa (14% NWP) leaked in the fire tests without rupture. Indeed, when initial pressure is substantially below NWP there is substantial "load+" wall thickness to be passed through by the resin decomposition front before it reaches the "reduced" load-bearing wall thickness fraction, and thus more time is available to melt the liner before the tank burst and thus initiate hydrogen release through the wall. These experimental observations are in line with the presented

simulations of the tank-TPRD system performance in the fire demonstrating melting of the liner and thus leakage through the wall before tank rupture. Results of a study of the effect of the state of charge (SoC) of a tank, i.e. reduced compared to NWP initial pressure, on the possibility of tank rupture in a fire will be described in a separate paper.

The experiments with three series of explosion free in a fire TPRD-less tank prototypes [24] demonstrated that if hydrogen leak through the wall starts after the liner melts then no tank rupture is observed. This could be explained by the expected increase of the leaking area of the wall as the wall thickness decreases significantly while the resin decomposition front propagates inwards. This innovative TPRD-less safety technology is out of the scope of this paper. Thus, we assume further in this study that after the liner melting the tank loses its tightness to hydrogen and no rupture of a tank will happen (see Fig. 8). This statement requires more experimental validation.

Figure 9a shows the hydrogen temperature in the tank that obeys the observed previously and presented above behaviour, i.e. temperature decreases after TPRD release start due to hydrogen expansion and then increases when the heat transfer through the tank wall takes over with some delay (about 5 min for this large volume tank).

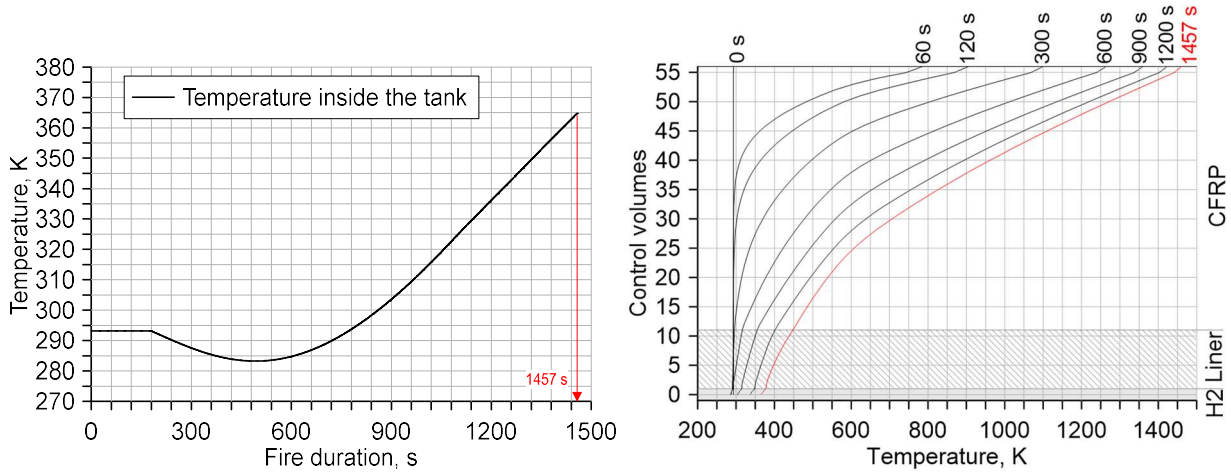

(a) (b)

Figure 10. (a) - hydrogen temperature dynamics in 244 L, 70 MPa tank during blowdown through TPRD=0.5 mm and TPRD activation delay of 180 s in HRR/A=1 MW/m^2 fire; (b) - temperature profiles in the tank wall, including the liner.

Figure 10b presents temperature profiles through the tank wall, including the liner, for the case of TPRD=0.5 mm for ten instances between the start of the fire and 1457 s (tank rupture time). The temperature of the tank surface (control volume 55) increases with time due to the fire. The temperature of the liner decreases at the beginning of the process due to the cooling of hydrogen during expansion. The heat flux from the fire propagates through CFRP, increases its temperature, then the liner temperature and starts to heat hydrogen after about 300 s of the release (about 480 s of the fire duration).

7.2. Case of 62.4 L tank-TPRD system

Let us consider the performance of a typical onboard hydrogen storage tank-TPRD system which includes a 62.4 L tank with two different TPRD diameters, i.e. 0.5 mm and 0.75 mm, with no TRPD activation delay and 3 min delay in a fire with HRR/A=1 MW/m^2 as in the previous case. Figure 11 shows the evolution of the resin decomposition front, the load-bearing wall thickness fraction, the pressure and the liner melting fronts in time.

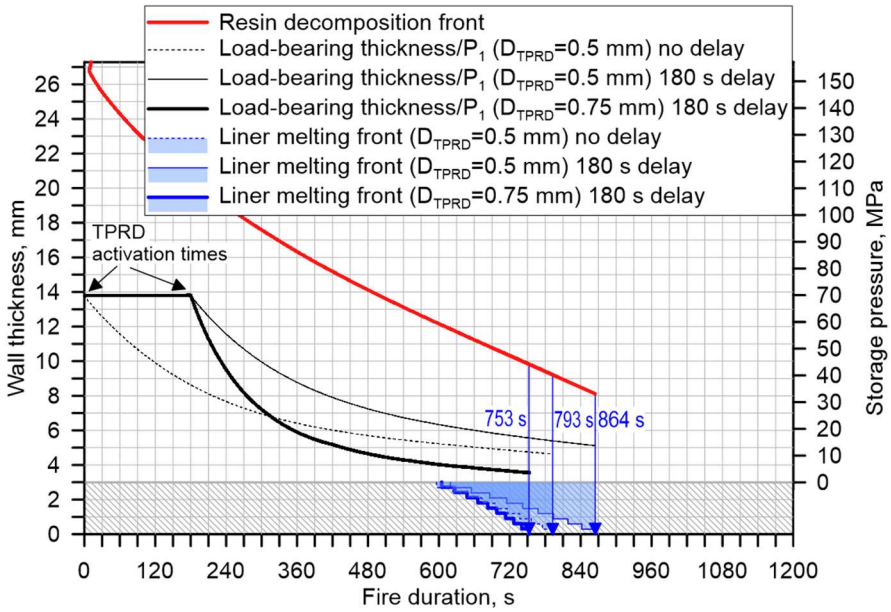

Figure 11. Performance of 62.4 L, 70 MPa tank-TPRD system in a fire with HRR/A=1 MW/m^2 for two different TPRD diameters (0.5 mm and 0.75 mm), and TPRD activation delay 0 s and 180 s.

For all three simulated scenarios, the liner melts long before the resin decomposition front would reach the reducing in time load-bearing wall thickness fraction. Thus, we could conclude that a TPRD diameter as small as 0.5 mm is enough to exclude 62.4 L, 70 MPa Type IV tank with HDPE liner rupture in a fire if TPRD is initiated within 3 min of the fire. The situation with TPRD=0.75 mm is inherently safer in sense of the tank rupture prevention. However, an increase of TPRD diameter would increase requirements to the garage minimum vent area to prevent its demolition by PPP (see section 7.5).

7.3. Case of 36 L tank-TPRD system

Figure 11 shows simulations of the thermal performance of the tank at the thinnest dome area of the 36 L, 70 MPa tank-TPRD system with the TPRD activation delay of 3 min for two different TPRD diameters 0.45 mm and 0.65 mm.

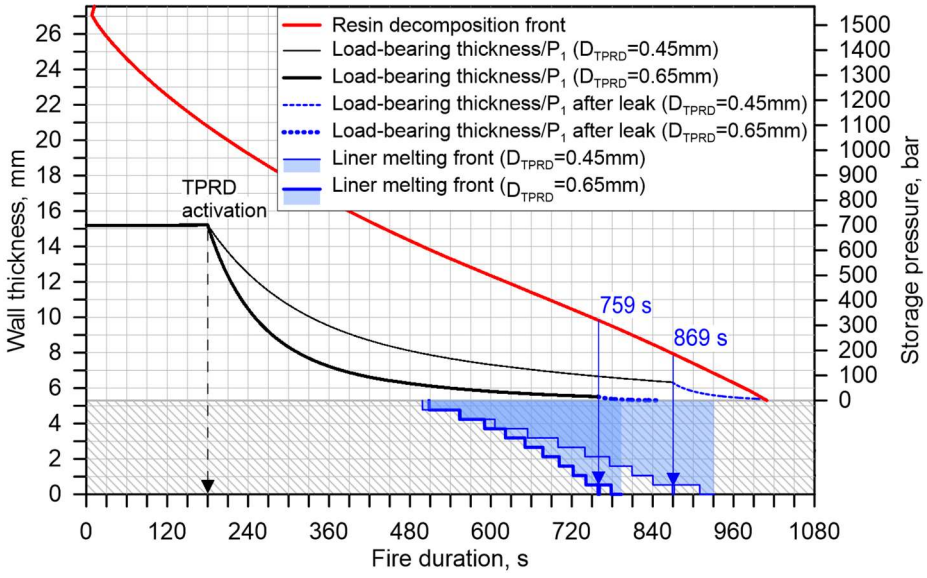

Figure 12. Performance of 36 L, 70 MPa tank-TPRD system in a fire with HRR/A=1 MW/m^2, for two different TPRD diameters (0.45 mm and 0.65 mm), and TPRD activation delay 180 s.

The analysis of these simulations is presented in the next section and includes the effect of the liner melting of the blowdown dynamics in the fire conditions.

7.4. The phenomenon of liner melting and its effect on the blowdown dynamics

It has been demonstrated above that a TRPD diameter of fractions of a millimetre is sufficient for hydrogen tank blowdown in a fire without rupture. It is shown that for tanks of storage capacities 244 L and 62.4 L the TPRD diameters 0.75 mm and 0.5 mm, respectively, can prevent tank rupture. The numerical study revealed the phenomenon of liner melting in the case of the use of TPRD of smaller diameter. The liner melting initiates microleaks of hydrogen through the composite wall which is not tight to hydrogen. This "additional" to the TPRD release of hydrogen assists the blowdown.

The explosion free in a fire TPRD-less tank of 7.5 L, 70 MPa is designed to leak through the wall after melting the liner. The fire testing of this innovative TPRD-less tank demonstrated the following. The leaks through the wall are in a form of microleaks. The equivalent diameter of these microleaks is changing at the final stage of the fire test from about 0.29 mm to about 0.70 mm at the end (at this stage pressure drops from around 15 MPa to the atmospheric pressure.

The studied in the previous section two numerical blowdowns in the fire of the 36 L tank-TPRD system showed (see Fig. 11) that liner melted for TPRD=0.45 mm at time 759 s when the pressure in the tank was 1.5 MPa, and for TPRD=0.65 mm at 869 s when pressure was 7.2 MPa. Because the leak in the first fire test was initiated at very low pressure we assume the equivalent leak diameter 0.7 mm, as per the final blowdown stage in the fire tests with TPRD-less tanks. In the second test, the "additional" leak through the wall after liner melting was initiated at pressure 7.2 MPa. Hence, an intermediate between 0.29 mm and 0.7 mm leak diameter of 0.495 mm can be assumed. To scale the leak equivalent area from 7.5 L to 36 L tank in the assumption that microleaks are equally distributed across the tank wall, we compare the ratio of the internal surface of 7.5 L and 36 L tanks. The internal surface area in the 7.5 L tank is 0.143 m^2 and it is 0.63 m^2 for the 36 L tank. The surface area ratio is then 0.63 m^2/0.143 m^2=4.41. We apply this scaling factor to the areas of equivalent leaks, i.e. leak through the equivalent diameter of 0.7 mm (test with TPRD=0.65 mm) and 0.495 mm (test with TPRD=0.45 mm) and then add them to the respective areas of TPRD. The new total increased release diameter is then 1.61 mm and 1.13 mm respectively. To represent the additional leak numerically, we switch from the initial TPRD orifice to the new increased diameter at the moment when the liner is fully melted. Bearing in mind that this is the theoretical study, the experimental validating of these results is needed.

Figure 11 shows that the case with TPRD=0.45 mm is naturally less "conservative" as the resin decomposition front and load-bearing wall thickness fraction are about 1.5 mm apart at 869 s when the liner is fully melted and the additional release (blue dash curve) was initiated. In this numerical fire test, the resin decomposition front meets the load-bearing wall thickness fraction (factually meaning "numerical rupture") at 1005 s when the tank pressure is only 578 kPa. The TPRD=0.65 mm test demonstrates for almost complete blowdown even before the liner melts at 759 s (tank pressure drops to 1.5 MPa). The "load+" thickness, in this case, remained almost 4 mm, and it can be seen that the additional leak through the wall provides a safe blowdown. In both simulated tests, we can observe the liner melting front slightly raises immediately after it was fully melted, and then descending again. This is due to the temperature decrease at the moment of starting the additional release through the wall (similarly to temperature dynamics in Fig. 7b). It also is worth noting, that the additional leak takes place when the pressure in the tank essentially reduced and thus it does not influence the PPP that is defined by the original TPRD diameter.

7.5. Requirements to TPRD diameter to exclude the pressure peaking phenomenon

It is highly unlikely that passenger cars would use onboard storage tanks with volume as large as 244 L. This means it is not necessary to consider the PPP in a garage [19]–[22] for tanks of large

volume such as 244 L. Thus, only 62.4 L and 36 L tank-TPRD systems are considered in this section concerning the PPP. Let us assume a residential garage of 30 m^3 volume. The pressure dynamics in the garage can be calculated using the PPP tool of the free access online e-Laboratory of Hydrogen Safety [59],[60] by application of the model for ignited release [20]. The garage vents of total size changing from one brick (50x250 mm) to four bricks (200x250 mm) are considered. Figure 13a and 12b show overpressure dynamics in the garage for releases from 62.4 L and 36 L tanks respectively for different TPRD diameters and different garage vent sizes.

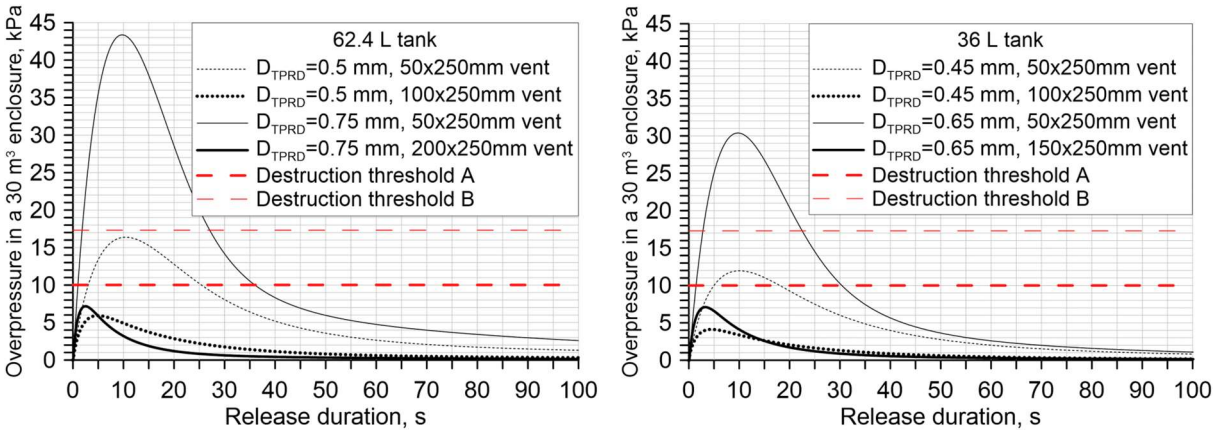

(a) (b)

Figure 13. The PPP overpressure dynamics in 30 m^3 garage and structural damage threshold A (10 kPa [17], [61]) and threshold B (17.3 kPa [62]): (a) - 62.4 L, 70 MPa tank-TPRD system; (b) - 36 L, 70 MPa tank-TPRD system.

The releases from 62.4 L tank through 0.5 mm and 0.75 mm TPRD diameters in the garage with one brick size (50x250 mm) give overpressures above 10 kPa (threshold A, [17],[61]). The increase of vent size to two bricks (100x250 mm) for TPRD=0.5 mm decreases the overpressure to an acceptable 6 kPa. Only four bricks vent (200x250 mm) is sufficient to reduce the PPP overpressure to an acceptable 7 kPa for TPRD=0.75 mm. As expected, TPRD=0.5 mm is preferable to TPRD=0.75 mm from the PPP point of view in low ventilation garages which are characteristic for cold climate locations (while both TPRDs prevent the tank rupture).

Figure 13b demonstrates that for a 36 L tank the overpressure is above threshold A of 10 kPa for both TPRD sizes if the garage vent size is equal to one brick area (50x250 mm). For TPRD=0.45 mm, the two bricks vent (100x250 mm) decreases the overpressure to an acceptable 4.2 kPa. For TPRD=0.65 mm, the three bricks vent area (150x250 mm) decreases the overpressure to an acceptable 7 kPa.

For hydrogen applications with onboard tanks of 70 MPa and volumes 36-62.4 L and HDPE liner, it is inherently safer to use TPRD diameters of 0.45-0.5 mm for blowdown in a fire to satisfy requirements for the prevention of the PPP consequences in a garage. However, it should be underlined that garages with vent size equal to or below one brick vent area (50x250 mm) can undergo negative consequences of the PPP and it is worth having a vent area of at least two brick vent size (100x250 mm).

CONCLUSIONS

The *originality* of this study is in the development of a comprehensive model of non-adiabatic thermal behaviour of a composite tank-TPRD system in a fire. The model accounts for the main underlying physical phenomena, including the composite resin thermal degradation and melting of the liner, etc. The phenomenon of liner melting during non-adiabatic blowdown of a tank through a reduced diameter of a TPRD orifice is revealed for the first time in the numerical experiments. The

"additional" leakage of hydrogen through the composite wall after the liner melting facilitates the inherently safer hydrogen blowdown from the tank in a fire.

The *significance* of the study is in the provision for the first time of the validated model and the methodology to design inherently safer tank-TPRD systems to prevent tank rupture in fires yet account for the mitigation of the pressure peaking phenomenon in a garage.
The universal dependence of the FRR decrease with the increase of HRR/A is established. The "asymptotic" minimum of FRR=4-6 min for investigated tanks is observed at HRR/A>1-2 MW/m^2 which is characteristic for gasoline/diesel fires. Fire test with lower HRR/A could artificially "increase" the FRR thus, allowing to pass the localised portion of the fire test. However, this could create serious safety concerns for public safety and property protection.

The FRR is an important parameter required by firemen to develop intervention strategies and tactics. The requirement of FRR experimental measurements, i.e. performing fire test without TPRD, must be added to the relevant regulations to account for the first responders' demand.
The exclusion of rupture of the studied Type IV tanks with NWP=70 MPa can be provided using a TPRD diameter of 0.75 mm for 244 L tank, 0.5 mm for 62.4 L tank, and 0.45 mm for 36 L tank. For releases in a garage from a passenger car (from onboard storage tanks 62.4 L and 36 L), at least two bricks total size vent area (100x250 mm) is needed to prevent the destructive consequences of the PPP on a structure.

The *rigour* of this study is in the model validation against experimental data on the blowdown of 19 L, 70 MPa Type IV tank with helium and 1 mm TPRD orifice, and the destructive fire test with 36 L, 70 MPa Type IV hydrogen tank with HDPE liner. The strength of the model is underpinned by the inclusion of all main physical phenomena affecting the complex process of heat and mass transfer during high-pressure hydrogen tank blowdown in fire conditions.

The dependence of FRR on HRR/A was built using experimental data, including tanks with NWP=35 MPa and 70 MPa of Type III and IV of different volumes and burners with different fuels. The developed model reproduces the experimental dependence of the FRR on the HRR/A.

ACKNOWLEDGEMENTS

The authors are grateful to the Engineering and Physical Science Research Council (EPSRC) of the UK for funding this work through the SUPERGEN Hydrogen and Fuel Cell Hub project (EP/P024807/1) and to Fuel Cells and Hydrogen 2 Joint Undertaking (FCH2 JU) for funding this research through the HyTunnel-CS project "Pre-normative research for safety of hydrogen driven vehicles and transport through tunnels and similar confined spaces" and SH2APED project "Storage of hydrogen: alternative pressure enclosure development". The HyTunnel-CS and SH2APED projects have received funding from the FCH2 JU under grant agreements No.826193 and No.101007182 respectively. This Joint Undertaking receives support from the European Union's Horizon 2020 research and innovation programme, Hydrogen Europe and Hydrogen Europe Research.

REFERENCES

[1] Yamashita A, Kondo M, Goto S, Oxgami N. Development of High-Pressure Hydrogen Storage System for the Toyota 'Mirai'. SAE Tech Pap 2015. https://doi.org/10.4271/2015-01-1169.

[2] Hexagon Composites Group. Hydrogen storage and transportation systems, https://www.hexagonxperion.com/fileadmin/user_upload/xperion_Energy___Environment/Datenblaetter_-_xperion_EE/Hexagon_xperion_Datenblaetter/Hydrogen-Solutions-flyer-February-2018.pdf; 2018 [accessed: 4 October 2020].

[3] Ferrara S, Kedzia K. MARANDA – Marine application of a new fuel cell powertrain validated in demanding arctic conditions 2017. Grant agreement No.735717. Deliverable 6.1: Storage system layout and design.
[4] United Nations Economic Commission for Europe. Global Registry. Addendum 13: Global technical regulation No. 13. Global technical regulation on hydrogen and fuel cell vehicles, http://www.unece.org/trans/main/wp29/wp29wgs/wp29gen/wp29glob_registry.html [accessed: 4 October 2020].
[5] United Nations Economic Commission for Europe. Addendum 133 – Regulation No. 134. Uniform provisions concerning the approval of motor vehicles and their components with regard to the safety-related performance of hydrogen fuelled vehicles (HFCV), https://www.unece.org/fileadmin/DAM/trans/main/wp29/wp29regs/2015/R134e.pdf [accessed: 4 October 2020].
[6] Commission Regulation. No 406/2010 implementing Regulation (EC) No 79/2009 of the Parliament and of the Council on type-approval of hydrogen-powered vehicles. Off J Eur Union 2010.
[7] IFD responds after trash truck's natural gas tanks explode, https://www.youtube.com/watch?v=CpmWPEhIaiU; 2016 [accessed 4 October 2020].
[8] A Garbage Truck Explosion Leaves Some Homes Damaged!, https://www.youtube.com/watch?v=9lxMWxq5zJE; 2016 [accessed 4 October 2020].
[9] CNG Tank Explodes Injuring School Bus Driver, https://www.youtube.com/watch?v=NfyUMWnhrBc; 2018 [accessed 4 October 2020].
[10] Ingason H, Li YZ. Spilled liquid fires in tunnels. Fire Saf J 2017;91:399–406. https://doi.org/10.1016/j.firesaf.2017.03.065.
[11] Ingason H, Li YZ, Lönnermark A. Tunnel Fire Dynamics. New York: Springer; 2015.
[12] Ingason H, Hammarström R. Fire test with a front wheel loader rubber tyre. SP Report 2010:64; 2010.
[13] Blanc-Vannet P. et al. Fire tests carried out in FCH JU Firecomp project, recommendations and application to safety of gas storage systems. Int J Hydrog Energy 2019;44:9100–9. https://doi.org/10.1016/j.ijhydene.2018.04.070.
[14] Weyandt N. Analysis of Induced Catastrophic Failure of A 5000 psig Type IV Hydrogen Cylinder. Southwest Research Institute report for the MVFRI; 2005.
[15] Kashkarov S, Makarov D, Molkov V. Effect of a heat release rate on reproducibility of fire test for hydrogen storage cylinders. Int J Hydrog Energy 2018;43:10185–92. https://doi.org/10.1016/j.ijhydene.2018.04.047.
[16] Dadashzadeh M, Kashkarov S, Makarov D, Molkov V. Risk assessment methodology for onboard hydrogen storage. Int J Hydrog Energy 2018;43:6462–75. https://doi.org/10.1016/j.ijhydene.2018.01.195.
[17] Molkov V. Fundamentals of hydrogen safety engineering. www.bookboon.com; 2012.
[18] Johnston IA. The Noble-Abel equation of state: Thermodynamic derivations for ballistic modelling, Weapons Systems Division Defence Science and Technology Organisation of Australian Government, Report DSTO–TN–0670, 2005. https://apps.dtic.mil/dtic/tr/fulltext/u2/a444005.pdf [accessed 15 January 2021].
[19] Hussein HG, Brennan S, Shentsov V, Makarov D, Molkov V. Numerical validation of pressure peaking from an ignited hydrogen release in a laboratory-scale enclosure and application to a garage scenario. Int J Hydrog Energy 2018;43:17954–68. https://doi.org/10.1016/j.ijhydene.2018.07.154.
[20] Makarov D, Shentsov V, Kuznetsov M, Molkov V. Pressure peaking phenomenon: Model validation against unignited release and jet fire experiments. Int J Hydrog Energy 2018;43:9454–9469. https://doi.org/10.1016/j.ijhydene.2018.03.162.

[21] Brennan S, Molkov V. Safety assessment of unignited hydrogen discharge from onboard storage in garages with low levels of natural ventilation. Int J Hydrog Energy 2013;38:8159–66. https://doi.org/10.1016/j.ijhydene.2012.08.036.
[22] Brennan S, Molkov V. Pressure peaking phenomenon for indoor hydrogen releases. Int J Hydrog Energy 2018;43:18530–41. https://doi.org/10.1016/j.ijhydene.2018.08.096.
[23] Gaseous hydrogen —Thermally activated pressure relief devices for compressed hydrogen vehicle fuel containers. ISO 19882:2018; 2018.
[24] Molkov V, Makarov D, Kashkarov S. Composite Pressure Vessel for Hydrogen Storage. WO 2018/149772 A1; 2018.
[25] Quang Dao D, Luche J, Richard F, Rogaume T, Bourhy-Weber C, Ruban S. Determination of characteristic parameters for the thermal decomposition of epoxy resin/carbon fibre composites in cone calorimeter. Int. J. Hydrog. Energy 2013; 38: 8167–78. https://doi.org/10.1016/j.ijhydene.2012.05.116.
[26] Dadashzadeh M, Makarov D, Kashkarov S, Molkov V. Non-adiabatic under-expanded jet theory for blowdown and fire resistance rating of hydrogen tank. In: International Conference on Hydrogen Safety (ICHS 2019), 24-26 September, Adelaide, Australia. Paper ID 182; 2019.
[27] Molkov V, Makarov D, Bragin M. Physics and modelling of underexpanded jets and hydrogen dispersion in atmosphere. Phys Extreme States Matter 2009;146–9.
[28] Patankar SV. Numerical heat transfer and fluid flow (Series in computational methods in mechanics and thermal sciences). New York: McGraw-Hill Book Company; 1980.
[29] Voller VR. A Heat Balance Integral Method for Estimating Practical Solidification Parameters. IMA J Appl Math 1985;35:223–32.
[30] Voller VR, Prakash C. A fixed grid numerical modelling methodology for convection-diffusion mushy region phase-change problems. Int J Heat Mass Transf 1987;30:1709–19.
[31] Voller VR. Development and application of a heat balance integral method for analysis of metallurgical solidification. Appl Math Model 1989;13:3–11.
[32] Voller VR, Brent AD, Prakash C. Modelling the mushy region in a binary alloy. Appl Math Model 1990;14:320–6.
[33] Wang S, Faghri A, Bergman TL. A comprehensive numerical model for melting with natural convection. Int J Heat Mass Transf 2010;53:1986–2000..
[34] Woodfield P L, Monde M, Mitsutake Y. Measurement of Averaged Heat Transfer Coefficient in High-Pressure Vessel during Charging with Hydrogen, Nitrogen or Argon Gas. J. Therm. Sci. Technol. 2007; 2: 180–91. https://doi.org/10.1299/jtst.2.180.
[35] Molkov V, Kashkarov S. Blast wave from a high-pressure gas tank rupture in a fire: Stand-alone and under-vehicle hydrogen tanks. Int J Hydrog Energy 2015;40:12581–603. https://doi.org/10.1016/j.ijhydene.2015.07.001.
[36] Monde M, Woodfield P, Takano T, Kosaka M. Estimation of temperature change in practical hydrogen pressure tanks being filled at high pressures of 35 and 70 MPa. Int J Hydrog Energy 2012;37:5723–34. https://doi.org/10.1016/j.ijhydene.2011.12.136.
[37] NIST. Isothermal properties for hydrogen, http://webbook.nist.gov/cgi/inchi?ID=C1333740&Mask=1#Thermo-Gas; 2017 [accessed 20 September 2020].
[38] Welch S, Hadden R. Hidalgo-Medina J, Pironi P. Thermal properties and thermal modelling of composite materials exposed to fires 2017, Bath, UK. SUPERGEN Challenge project meeting, Bath, UK; 2017.
[39] Liu W, Varley RJ, Simon GP. Understanding the decomposition and fire performance processes in phosphorus and nanomodified high performance epoxy resins and composites. Polymer 2007;48:2345–2354.

[40] Acosta B, Moretto P, de Miguel N, Ortiz R, Harskamp F, Bonato C. JRC reference data from experiments of on-board hydrogen tanks fast filling. Int J Hydrog Energy 2014;39:20531–37. https://doi.org/10.1016/j.ijhydene.2014.03.227.
[41] Monde M, Kosaka M. Understanding of Thermal Characteristics of Fueling Hydrogen High Pressure Tanks and Governing Parameters. SAE Int J Altern Powertrains 2013;2:61–67. https://doi.org/10.4271/2013-01-0474.
[42] Hidalgo JP, Pironi P, Haden RM, Welch S. Effect of Thickness on the Ignition Behaviour of Carbon Fibre Composite Materials Used in High Pressure Vessels. In: Proc. of the Eighth International Seminar on Fire & Explosion Hazards (ISFEH8), 25-28 April, Hefei, China; 2016.
[43] NIST. Isothermal properties for helium, http://webbook.nist.gov/cgi/fluid.cgi?T=293&PLow=0&PHigh=70&PInc=&Applet=on&Digits=5&ID=C7440597&Action=Load&Type=IsoTherm&TUnit=K&PUnit=MPa&DUnit=mol%2Fl&HUnit=kJ%2Fmol&WUnit=m%2Fs&VisUnit=uPa*s&STUnit=N%2Fm&RefState=DEF; 2017 [accessed 20 September 2020].
[44] Chenoweth DR. Gas-transfer analysis. Section H-Real gas results via the van der Waals equation of state and viral-expansion extensions of its limiting Abel-Noble form. Sandia report. Livermore, CA; 1983.
[45] The Engineering ToolBox. Resources, tools and basic information for engineering and design of technical applications, http://www.engineeringtoolbox.com/index.html; 2017 [accessed 20 September 2020].
[46] Makarov D, Kim Y, Kashkarov S, Molkov V. Thermal protection and fire resistance of high-pressure hydrogen storage. In: Proc. of the Eighth International Seminar on Fire & Explosion Hazards (ISFEH8), 25-28 April, Hefei, China; 2016.
[47] Heggem P. Private communication; 2013.
[48] Kashkarov S, Makarov D, Molkov V. Model of 3D conjugate heat transfer and mechanism of compressed gas storage failure in a fire. International Conference on Hydrogen Safety (ICHS 2017), 24-26 September, Hamburg, Germany, Paper ID 125; 2017.
[49] MatWeb Material Property Data. Overview of materials for High Density Polyethylene (HDPE), Pipe Grade; http://www.matweb.com/search/DataSheet.aspx?MatGUID=c305addb2e1c4a58a3dece14122acfde; 2018 [accessed 28 August 2017].
[50] Hu J, Chen J, Sundararaman S, Chandrashekhara K, Chernicoff W. Analysis of composite hydrogen storage cylinders subjected to localized flame impingements. Int J Hydrog Energy 2008;33:2738–46.https://doi.org/10.1016/j.ijhydene.2008.03.012.
[51] Saldi Z, Wen J. Modeling thermal response of polymer composite hydrogen cylinders subjected to external fires. Int J Hydrog Energy 2017;42:7513–20. https://doi.org/10.1016/j.ijhydene.2016.06.108.
[52] Sapre S, Pareek K, Vyas M. Investigation of structural stability of type IV compressed hydrogen storage tank during refueling of fuel cell vehicle. Energy Storage 2020;2:e150. https://doi.org/10.1002/est2.150.
[53] Weyandt N. Vehicle bonfire to induce catastrophic failure of a 5000-psig hydrogen cylinder installed on a typical SUV. Southwest Research Institute report for MVFRI; 2006.
[54] S Ruban S. et al. Fire risk on high-pressure full composite cylinders for automotive applications. Int J Hydrog Energy 2012;37:17630-8. https://doi.org/10.1016/j.ijhydene.2012.05.140.
[55] Bustamante Valencia L, Blanc-Vannet P, Heudier L, Jamois D. Thermal history resulting in the failure of lightweight fully-wrapped composite pressure vessel for hydrogen in a fire

experimental facility. Fire Technology 2016;52:421–42. https://doi.org/10.1007/s10694-015-0513-y.
[56] Olson M. Private communication. 2020.
[57] Mattelaer V. Private communication. 2018.
[58] Halm D, Fouillen F, Laine E, Gueguen M, Bertheau D, Van Eekelen T. Composite pressure vessels for hydrogen storage in fire conditions: Fire tests and burst simulation. Int J Hydrog Energy 2017;42:20056–70. https://doi.org/10.1016/j.ijhydene.2017.06.088.
[59] e-Laboratory, https://fch2edu.eu/home/e-laboratory/ [accessed 23 January 2021].
[60] Shentsov V, Makarov D, Molkov V. Scientific Principles of e-Laboratory of Hydrogen Safety. In: Proc. of the Ninth International Seminar on Fire & Explosion Hazards (ISFEH9), 21-26 April 2019, Saint Petersburg, Russia.
[61] W Baker WE, Cox PA, Westine PS, Kulesz JJ, Strehlow RA. Explosion hazards and evaluation. Elsevier Scientific Publishing Company; 1983.
[62] HSE. The Peterborough Explosion. A report of the investigation by the Health and Safety Executive into the explosion of a vehicle carrying explosives at Fengate Industrial Estate, Peterborough on 22 March 1989. Report; 1990.